JOURNAL OF GEOPHYSICAL RESEARCH, VOL. 111, B12S05, doi:10.1029/2006JB004561, 2006

Low-temperature magnetic behavior of multidomain titanomagnetites: TM0, TM16, and TM35

Brian Carter-Stiglitz,[1] Bruce Moskowitz,[1] Peter Solheid,[1] Thelma S. Berquó,[1] Michael Jackson,[1] and Andrey Kosterov[1]

Received 13 June 2006; revised 21 September 2006; accepted 11 October 2006; published 9 December 2006.

[1] An unpredicted effect of the Verwey transition in magnetite is that a field-cooled (FC) remanent magnetization can be less intense than a zero-field cooled (ZFC) isothermal remanence. The effect, only documented in a handful of multidomain (MD) samples, is thought to be unique to MD material. Data for new MD samples all show an elevation of ZFC over FC remanences. Current theory suggests that the FC easy axis bias alone produces the effect. We measured hysteresis loops after three cooling pretreatments; the results are inconsistent with the aforementioned theory. They are, however, consistent with a previous hypothesis which cites the absence of transformational twins in FC samples as an important factor. Our initial low-temperature domain observations in FC and ZFC magnetite further support this theory. We also present data for MD titanomagnetites (x = 0.16, 0.35). These samples also show elevated ZFC remanences below a critical temperature (T_{crit}). The titanomagnetites' frequency dependence of susceptibility around T_{crit}, the suppression of the amplitude dependence of susceptibility below T_{crit}, and Mössbauer data suggest that the change in magnetic anisotropy at T_{crit} is related to a suppression of B site electron hopping at low temperature, at least on the timescale of the magnetic measurements. Given our remanence data, field cooling must affect the orientation of the new low-temperature magnetic easy axis. We appeal to the same process as we did for magnetite to explain the elevation of ZFC moments, noting that the exact nature of the transition across T_{crit} is not completely understood.

Citation: Carter-Stiglitz, B., B. Moskowitz, P. Solheid, T. S. Berquó, M. Jackson, and A. Kosterov (2006), Low-temperature magnetic behavior of multidomain titanomagnetites: TM0, TM16, and TM35, *J. Geophys. Res.*, *111*, B12S05, doi:10.1029/2006JB004561.

1. Introduction

[2] Beginning with the pioneering work of *Ozima et al.* [1964], *Nagata* [1965], and *Creer and Like* [1967], low-temperature (4.2–300 K) magnetic experiments have successfully answered numerous questions in the geosciences. Over the past decade we have gleaned a much better understanding of the mechanisms controlling the low-temperature magnetic behavior of geologically important magnetic minerals [*Rochette et al.*, 1990; *Moskowitz et al.*, 1993; *Özdemir et al.*, 1993; *Muxworthy and McClelland*, 2000; *Carter-Stiglitz et al.*, 2002; *Kosterov*, 2002; *Özdemir et al.*, 2002]. This enables the use of low-temperature magnetometry to identify and quantify trace amounts (<100 ppm) of target minerals [*Jackson et al.*, 1993; *Roberts et al.*, 1995; *Torii et al.*, 1996; *Bogalo et al.*, 2001], and nanophase (<30 nm) material [*Banerjee et al.*, 1993; *Eyre and Shaw*, 1994; *Hunt et al.*, 1995; *Tarduno*, 1995; *Dearing et al.*, 1997; *Passier et al.*, 2001].

[3] The bulk of the low-temperature rock magnetic research conducted to date concerns magnetite, which undergoes two important low-temperature transitions. A structural phase transition, the Verwey transition, occurs near 120 K (T_v) and a magnetic transition, the isotropic point, occurs near 130 K where the cubic magnetocrystalline easy axis switches from the body diagonal to the cube edge [e.g., *Dunlop and Özdemir*, 1997]. Although the change in saturation isothermal remanence (SIRM) at T_v has been used most often as a simple magnetic fingerprint of magnetite (and is now a standard tool in paleomagnetism and environmental magnetism), research has also discovered that particle size, remanence type (weak field versus strong field), and cooling treatments affect the magnetic response to the Verwey transition and the isotropic point in several intriguing ways. Examples include the following: (1) the amount of remanence lost on warming through T_v increases with increasing grain size [*Özdemir et al.*, 1993; *Halgedahl and Jarrard*, 1995; *Özdemir et al.*, 2002]; (2) the partial recovery of a remanence imparted at 300 K, when cooled and warmed in a 300→10→300 K cycle decreases with increasing grain size with single domain (like) states having the highest memory [*Dunlop and Argyle*, 1991; *Hodych*, 1991; *Heider et al.*, 1992; *Halgedahl and Jarrard*,

[1]Institute for Rock Magnetism, Newton Horace Winchell School of Earth Sciences, University of Minnesota, Minneapolis, Minnesota, USA.

0148-0227/06/2006JB004561$09.00

1995; *Shcherbakova et al.*, 1996; *King and Williams*, 2000; *Özdemir et al.*, 2002]; (3) in multidomain grains, strong-field remanence, e.g., SIRM, decreases more rapidly as T_v is approached on cooling than weak-field remanences, e.g., thermoremanent magnetization (TRM) [*Muxworthy and Williams*, 1999; *Muxworthy and McClelland*, 2000; *Özdemir et al.*, 2002]; and (4) cooling through T_v in a magnetic field has a large effect on the magnetic properties of magnetite below T_v as well as the change in magnetic properties on warming through T_v. The data and analysis presented address this last phenomenon as it affects MD grains.

[4] On cooling through T_v one of the cube edges of the cubic phase becomes the monoclinic *c* axis, the magnetocrystalline easy axis. The *a* and *b* axes are then defined by two orthogonal face diagonals, which are the hard and intermediate magnetic axes, respectively. There is a slight rhombohedral elongation of the *c* axis in the direction of *a*, with $\beta = 90.23°$. The structural transition also results in transformational twinning below T_v, where any of the three cubic edges are likely twin variants for the monoclinic *c* axis. This twinning can be reduced or eliminated by cooling through the transition in a field, which restricts the *c* axis to the cube edge that is closest to the applied field, resulting in an easy axis bias [*Li*, 1932].

[5] Work on the low-temperature magnetism of titanomagnetites has been much more limited than that for magnetite. The low-temperature magnetocrystalline anisotropy and magnetostriction for titanomagnetites have, however, been characterized [*Syono*, 1965; *Kakol et al.*, 1991b]. *Radhakrishnamurty and Likhite* [1993] documented the temperature and frequency dependence of susceptibility for a suite of titanomagnetites. The samples encompassed the entire solid solution with a grain size of $\sim$20 μm. They observed peaks in susceptibility apparently associated with isotropic points, as well as a curious frequency dependence of susceptibility at low temperature for which they did not put forth an explanation. *Moskowitz et al.* [1998] characterized the low-temperature variation of magnetic susceptibility, at a single frequency and amplitude, and measured ZFC saturation remanences on warming for a large set of single crystal samples spanning TM0-TM60. They found that the character of the thermomagnetic curves were largely governed by the temperature variation of magnetocrystalline anisotropy and electronic and lattice relaxation effects. *Schmidbauer and Readman* [1982] measured ZFC and FC hysteresis loops for Ti-rich titanomagnetites, from TM40 to TM80. Their results indicated a change in grain-scale magnetic anisotropy (e.g., magnetocrystalline) below some critical temperature (T_{crit}) to a uniaxial anisotropy that is much harder than that above T_{crit}. Moreover, they found that field cooling affected the alignment of the new easy axis producing square hysteresis loops when measured parallel to the cooling field. They also observed FC remanences elevated over ZFC ones.

[6] Numerous studies of the magnetic after affect have also been conducted on magnetites and titanomagnetites. In such studies the time dependence of susceptibility is measured after alternating field demagnetization. The time dependence is measured as a function of temperature; typically, a self-hardening, i.e., a decrease of susceptibility with time, is observed to a varying degree as a function of temperature [*Walz et al.*, 1997]. Of particular importance to the results discussed in this study is the time dependency observed in both magnetite and titanomagnetites for 50 K < T < 100 K which is suggested to be related to thermally activated electron hopping between Fe^{+2} and Fe^{+3} [*Walz et al.*, 1997]. In magnetite a time dependence of susceptibility is also observed at lower temperatures, T < 35 K, and is thought to be caused by electron tunneling [*Kronmüller et al.*, 1974].

2. Samples and Experimental Methods

2.1. Magnetic Techniques

[7] Hysteresis loops (measured at 300 K and 20 K), and saturation magnetization (σ_s) as a function of temperature were measured using a Princeton Measurements Corp. vibrating sample magnetometer housed at the Institute for Rock Magnetism, University of Minnesota. Low-temperature remanence and susceptibility measurements were made using a Magnetic Properties Measurement System susceptometer manufactured by Quantum Design. Remanence was measured on warming from 10 to 300 K starting from two initial states: zero-field cooled (ZFC) from 300 K to 10 K after which a saturating field of 2.5 T was applied; and field cooled (FC) in 2.5-T field. Susceptibility was measured during warming from 10 to 300 K at 7 frequencies (1–1000 Hz) and 5 field amplitudes (16–240 A/m). Mössbauer spectra were measured at room temperature and at 4.2 K using a conventional constant acceleration spectrometer in transmission geometry with a ^{57}Co/Rh source, and using α-Fe at room temperature to calibrate isomer shifts and velocity scale.

2.2. Low-Temperature Domain Imaging

[8] *Smith et al.* [1980] developed a domain observation method that can be employed at variable temperature. The technique, the dry Bitter method, evaporates a small amount of Fe in a He atmosphere of $\sim$133 Pa. As the Fe moves away from the filament it condenses into nanoparticles ($\sim$10–50 nm) of iron. The iron particles are then deposited on the surface of the sample which is some centimeters away. Given that the particles are traveling slowly enough, they are, just as in the traditional Bitter method, attracted to locations with stray magnetic fields. Once deposited the particles remain immobile unless physically disturbed. The sample is then allowed to return to ambient temperature and the deposited pattern is observed optically or using electron microscopy. The apparatus that we used was a modified version of that used by *Smith et al.* [1980]. We used a field emission gun scanning electron microscope, JEOL model 6500, to image the domain patterns.

[9] There are five essential variables that control the quality, in terms of domain observation, of a given deposition: the current in the filament; the time the current is present; the distance between the filament and the sample; the amount of Fe on the filament; and the He pressure in the chamber. If any one of these variables is not optimized for pattern formation the experiment fails. Four modes of failure seem to be present: a thin film may be deposited, instead of a carpet of small particles; too little material may be deposited; too much material may be deposited; and the particles may be moving too quickly and deposit on the

Table 1. Hysteresis Properties[a]

Sample	T, K	Cooling	σ_s, A m^2/kg	σ_r/σ_s	$\mu_0 H_c$, mT
W041183	300	n/a	94	0.078	4.7
	10[b]	ZFC	—	0.100	14.2
	10	$FC_{\|}$	—	0.072	8.7
	10	$FC_{\perp}$	—	0.070	13.6
W112982	300	n/a	92	0.059	3.0
	10	ZFC	—	0.108	7.2
	10	$FC_{\|}$	—	0.086	5.3
	10	$FC_{\perp}$	—	0.082	6.8
AV5A3	300	n/a	0.5	0.014	1.1
	10	ZFC	—	0.050	8.5
	10	$FC_{\|}$	—	0.027	4.1
	10	$FC_{\perp}$	—	0.030	7.6
PT1B3	300	n/a	2.7	0.025	3.4
	10	ZFC	—	0.029	8.0
	10	$FC_{\|}$	—	0.021	5.0
	10	$FC_{\perp}$	—	0.029	9.7
TMBJ16_1	300	n/a	70	0.043	1.4
TMBJ35_1	300	n/a	50	0.054	1.9

[a]T is the temperature at which the loop was measured, σ_s is the saturation magnetization, σ_r is the saturation remanent magnetization, and H_c is the coercivity; n/a, not applicable.
[b]Mass was not measured for low-temperature specimens.

surface unaffected by the stray magnetic fields. Thermal convection currents in the chamber (driven by the hot filament and the cold sample) are sufficiently different between a room temperature deposition and a low-temperature deposition to ensure that the same set of conditions may fail in one case but succeed in the other.

2.3. Samples

[10] Four multidomain magnetite samples were characterized in this study: two synthetic samples produced by Wright industries W041183 (30–40 μm [*Jackson et al.*, 1990], 20.1 ± 13.4 μm [*Yu et al.*, 2002]) and W112982 (37.5 μm [*Jackson et al.*, 1990], 18.6 ± 9.6 μm [*Yu et al.*, 2002]), and two whole rock samples, a granite (AV5A3) and a gabbro (PT1B3) [*Brachfeld et al.*, 2002]. The two powder samples were dispersed in CaF_2. All four samples show clear multidomain hysteresis behavior, with low remanence ratios, low coercivities, and ramp-shaped hysteresis loops (Table 1). The lower remanence ratios and coercivities of AV5A3 and PT1B3 indicate that they contain much coarser grains than the two synthetic samples. The whole rock samples had Curie temperatures, deduced from σ_s measured in the temperature range of 20–700°C and using the two-tangent method, consistent with magnetite. AV5A3 yielded a Curie temperature of 585°C on warming and 580°C on cooling, and PT1B3B yielded 587°C and 582°C respectively. Mössbauer spectra for the Wright samples showed the presence of two sextets, representing the typical A and B sites, and indicated near stochiometric magnetite for both samples.

[11] We also manufactured two samples of randomly oriented multidomain grains of titanomagnetite with compositions of x = 0.16 and x = 0.35 (where x is defined in the formula: $Fe_{3-x}Ti_xO_4$ and was deduced from the Curie temperatures), TM16BJ_1 and TM35BJ_1, respectively. The samples were made in the following manner. ~1 mm thick discs were cut from the rod-shaped single crystals prepared by *Wanamaker and Moskowitz* [1994]. We then ground the discs into a powder using a mortar and pestle. The grain size distributions of the powders were characterized using a Horiba LA-920 laser diffraction grain size analyzer. The lognormal distributions' mean, median, mode, and standard deviation were respectively: 18 μm, 17 μm, 21 μm, and 9 μm for TM16BJ_1; and 33 μm, 32 μm, 42 μm, and 16 μm for TM35BJ_1. The samples were dispersed in CaF_2 before magnetic characterization. Hysteresis loops for the two samples were typical of MD material (Table 1), and the samples had reversible Curie temperatures of 480°C, and 365°C, for TM16BJ_ 1 and TM35BJ_ 1, respectively.

[12] For the low-temperature domain observations we experimented on a ~1 cm natural single crystal of magnetite, with a Verwey transition temperature of 118 K. Samples were cut to produce a (100) surface and then polished with diamond grit and colloidal silica.

3. Results

3.1. Low-Temperature Remanence: Magnetite, TM16, and TM35

[13] The ZFC and FC remanence data for the four MD magnetites are remarkably similar (Figures 1a–1d). ZFC remanences are ~50% larger than FC remanences. The low-temperature remanences are fairly stable on warming to T_v, demagnetizing by only ~10%. At T_v both ZFC and FC remanences almost completely demagnetize, and hence yield delta ratios [see, *Moskowitz et al.*, 1993] near 1. The elevation of ZFC remanences over FC remanences below T_v appears to be a unique signature of MD (titano)magnetite [e.g., *Brachfeld et al.*, 2001, 2002; *Kosterov*, 2003]. The behavior is opposite to that observed in SSD magnetite [*Moskowitz et al.*, 1993; *Carter-Stiglitz et al.*, 2002]. Notably W041183 shows less remanence decay on warming to T_v than the other three samples.

[14] The ZFC remanences for the two titanomagnetites are also elevated over the FC remanences. Like the magnetite, this elevation persists until a precipitous drop in magnetization at a critical temperature. For TM16BJ_1 T_{crit} ~50 K. TM35BJ_1 has a large drop at 50 K as well, but also a subsequent drop at ~125 K. The elevation of ZFC remanence persists up to the higher critical temperature. Although it is tempting to suggest that the higher-temperature loss is due to magnetite contamination in the sample, we do not think this is the case. TM35BJ_1 yields a single Curie point, and the same critical temperature has been noted in two previous studies for samples with similar compositions [*Schmidbauer and Readman*, 1982; *Moskowitz et al.*, 1998]. We also note that *Schmidbauer and Readman* [1982] (for their sample of TM40) did not observe an elevation of ZFC remanence over the FC one, but rather the opposite. We do not have a complete explanation for this discrepancy but note that they used a weaker applied field which might have resulted in undersaturation of the ZFC remanences.

3.2. Low-Temperature Hysteresis Loops: Magnetite

[15] Hysteresis loops were measured on the four MD magnetite samples at 20 K after zero-field cooling and field cooling in a 1.5 T field. In both cases loops were measured in two orientations: (1) parallel to the cooling field direction, denoted $FC_{\|}$, and (2) perpendicular to the cooling field, denoted $FC_{\perp}$ (Figures 2 and 3).

[16] Three of the samples show, broadly, the same hysteresis behavior: W041183, AV5A3, and PT1B3B. ZFC

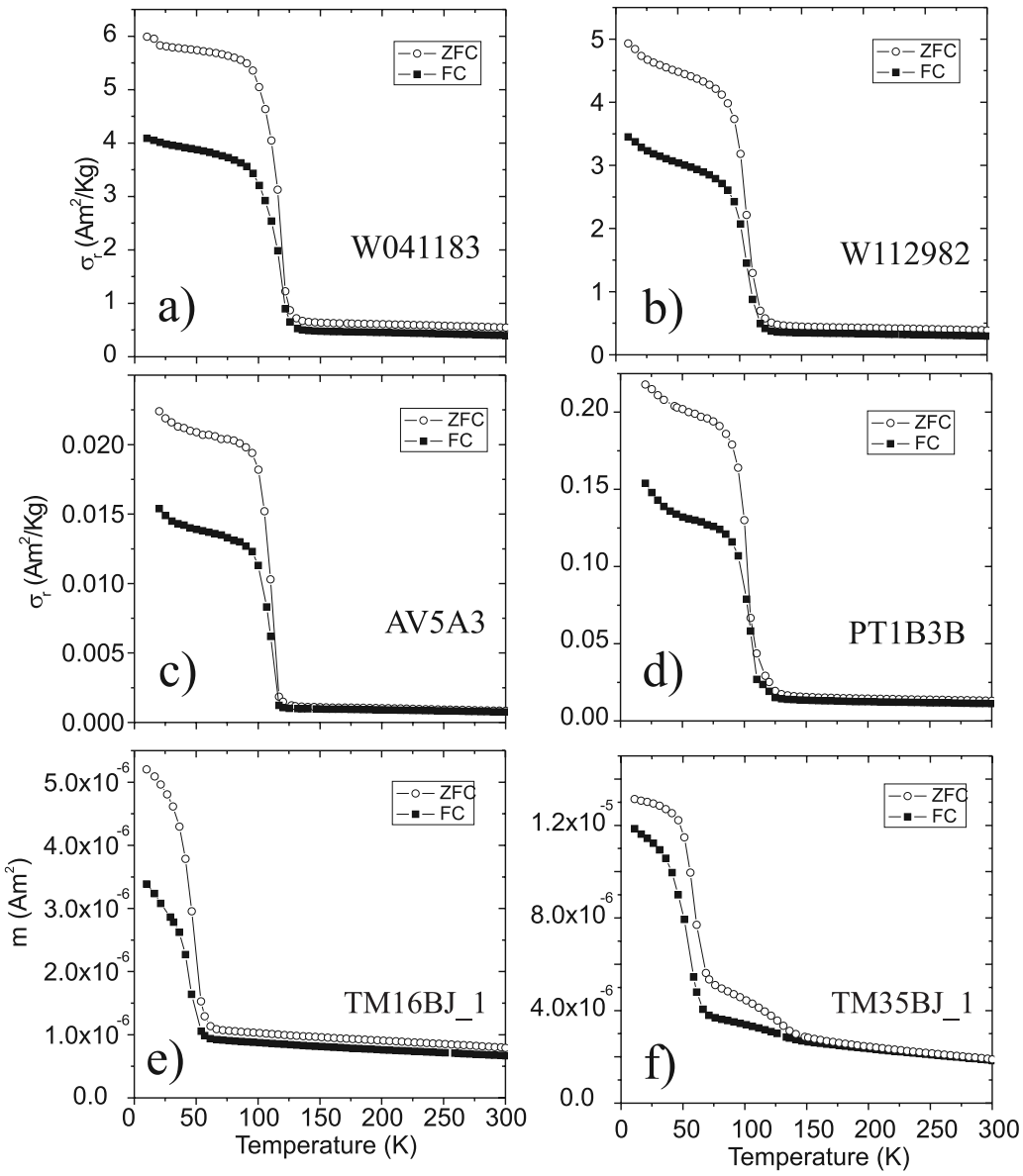

Figure 1. Low-temperature remanent magnetization measured on warming after zero-field cooling and field cooling for (a) W041183, (b) W112982, (c) AV5A3, (d) PT1B3B, (e) TM16BJ_1, and (f) TM35BJ_1.

hysteresis loops are nearly isotropic, whereas FC loops are anisotropic. The slight anisotropy of the ZFC hysteresis loops for the whole rock samples can be explained by a heterogeneous distribution of magnetic material in the samples. Judging by the approach to saturation the $FC_{\|}$ loops are the magnetically "softest" of the three cases (ZFC, $FC_{\|}$, and $FC_{\perp}$), followed by the ZFC case. The $FC_{\perp}$ are the magnetically "hardest" of the hysteresis loops (Figure 2a, 3a, and 3c). Interestingly this relationship does not hold for the coercivity, which is nearly equal for the ZFC and $FC_{\perp}$ cases, but much less for the $FC_{\|}$ case (Figures 2b, 3b, and 3d).

[17] For all samples, the ZFC remanence ratio is significantly higher than the FC remanence ratios, and the FC remanence ratios are basically equal for the parallel and perpendicular cases. For PT1B3 the $FC_{\perp}$ remanence ratio is somewhat elevated over the $FC_{\|}$ one. The elevation is, however, comparable to the difference in remanence ratios of the two ZFC loops.

[18] The loops measured on W112982 show some significant differences in comparison to the other three samples (Figures 2c and 2d). The $FC_{\|}$ case is again the softest of the low-temperature loops, but for this sample the ZFC case yields the hardest loops, in terms of approach to saturation. The ZFC case also has the largest coercivity and remanence ratio, with the two FC cases having essentially the same coercivities and remanence ratio.

3.3. Susceptibility as a Function of Temperature, Frequency, and Amplitude: TM16 and TM35

[19] Here we only show susceptibility data for the titanomagnetite samples, as the data for our magnetite samples were entirely consistent with those shown previously [*Moskowitz et al.*, 1998; *Skumryev et al.*, 1999; *Kosterov*, 2003].

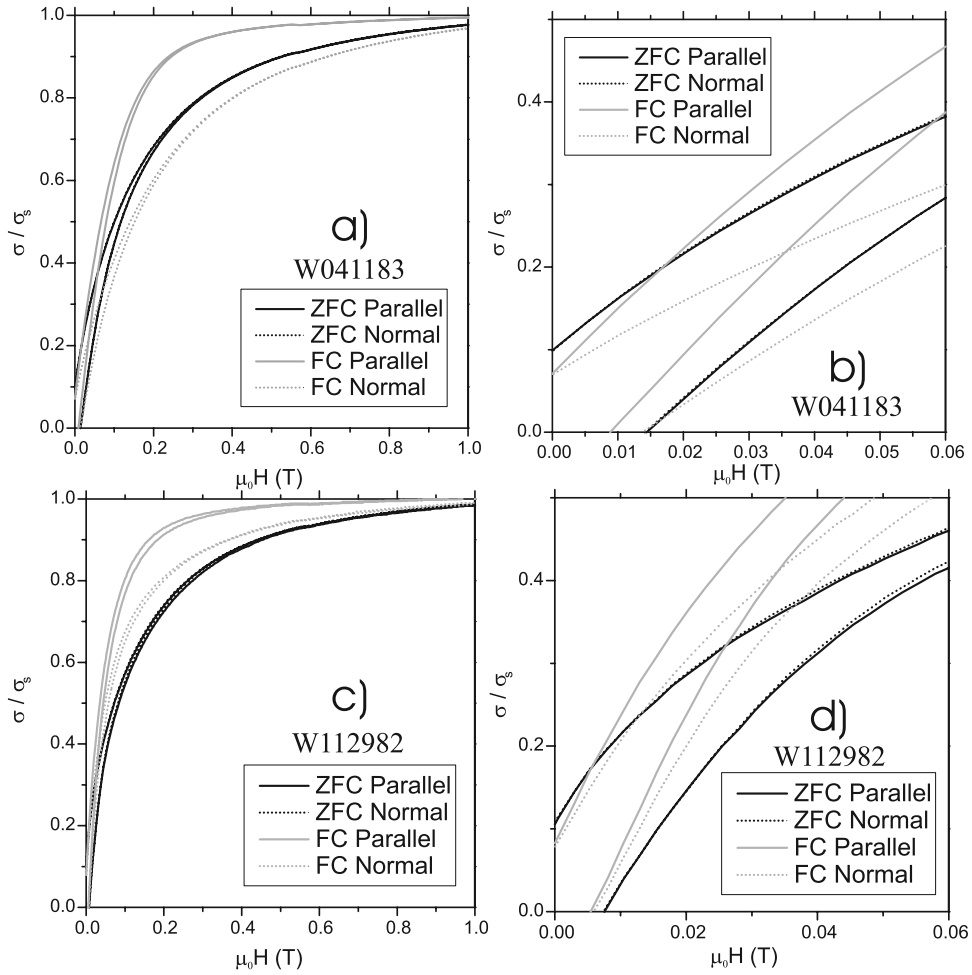

Figure 2. Hysteresis loops (maximum field is 1.5 T) measured at 20 K after zero-field cooling and field cooling both parallel (solid lines) and perpendicular (dashed lines) to the cooling field direction for (a, b) W041183 and (c, d) W112982.

Specifically, we note the same enhancement of the frequency dependence of susceptibility for $T < T_v$ with field cooling as observed by *Kosterov* [2003].

[20] Both titanomagnetite samples manifest very similar behavior. The susceptibilities drop steeply on cooling; the temperature of the drop decreases with decreasing frequency producing a frequency dependence of susceptibility below ~100 K and ~150 K for TM16 and TM35, respectively (Figures 4a and 4b). These are similar to the results of *Radhakrishnamurty and Likhite* [1993]. At the lowest frequency, the temperatures of the susceptibility drops approach the critical temperatures observed in the remanence measurements (Figures 1e, 1f, 4a, and 4b). Above the drop in susceptibility a strong amplitude dependence of susceptibility is observed (Figures 4c and 4d). This dependence is due to low-field hysteresis previously documented in titanomagnetites at room temperature [*Jackson et al.*, 1998].

4. Discussion

4.1. Magnetite

[21] One of the most perplexing aspects of the low-temperature behavior of MD magnetite is that the remanence imparted by field cooling (300–10 K) in a 2.5-T field is weaker than the low-temperature remanence acquired after zero field cooling [*Brachfeld et al.*, 2001; *Carter-Stiglitz et al.*, 2001; *Kosterov*, 2001, 2003]. Phenomenologically, this behavior seems to be unique to MD (titano)magnetite. Moreover, this behavior is opposite to that of SSD and small PSD magnetite (<1 μm), which have elevated FC remanences due to the easy axis bias induced by the cooling field.

[22] *Kosterov* [2003] suggested that the geometry of the distributions of easy axes accounts for the difference in ZFC and FC behavior in MD magnetite. Figures 5a and 5b show modeled distributions of *c* axis directions in the ZFC and FC states for a sample of randomly oriented grains. The easy axis bias for the FC sample reduces the energy taken to align the magnetizations with the applied field, thus explaining the observation that the FC samples are magnetically softer than the ZFC. To explain the elevation of the ZFC remanences over FC remanences *Kosterov* [2003] put forth the following argument: the microcoercivity due to domain wall displacement is expected to vary as sec(θ), where θ is the angle between the applied field and the magnetization within a domain. For an assemblage of grains, the higher the average angle between the magnetic easy axis and the

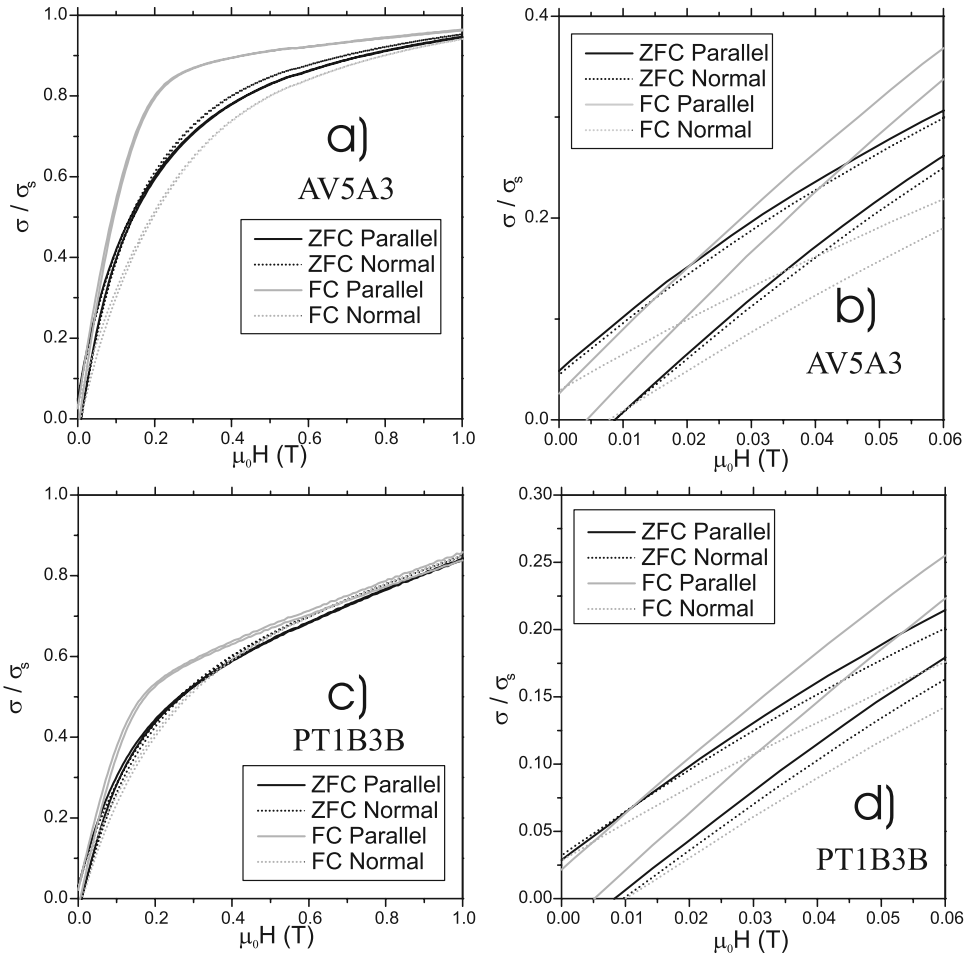

Figure 3. Hysteresis loops (maximum field is 1.5 T) measured at 20 K after zero-field cooling and field cooling both parallel (solid lines) and perpendicular (dashed lines) to the cooling field direction for (a, b) AV5A3 and (c, d) PT1B3B.

applied field, the higher the bulk coercivity. Moreover, for MD grains, saturation remanence is linearly related to coercivity through the demagnetizing factor [e.g., *Dunlop and Özdemir*, 1997]. Thus SIRM increases with increasing H_c. Consider the ZFC and $FC_{\parallel}$ cases. The average angle between the easy axis and the applied field is clearly higher in the ZFC case than in the $FC_{\parallel}$ case (Figures 5a and 5b). According to the model, the coercivity in the ZFC case is higher and so is the remanence. Extending this model, consider the $FC_{\perp}$ case. It has the largest average angle between magnetocrystalline easy axis and applied field (Figure 5a–5c), and should therefore have both the highest coercivity and the largest remanence. In summary, the model predicts that magnetic hardness, in terms of approach to saturation and H_c, increases in the following order: $FC_{\parallel} < ZFC < FC_{\perp}$, and the same relationship holds for saturation remanence.

[23] This geometric model, on its own, is deficient in the following ways. First, the prediction that the $FC_{\perp}$ case is always harder than the ZFC case is contradicted by W112982 in terms of the approach to saturation and H_c (Figures 2c–2d), and by the other three MD samples in terms of H_c (Figures 2b, 2d, 3b, and 3d). For these three samples H_c is approximately the same for both the ZFC and $FC_{\perp}$ cases. Second, the prediction that the $FC_{\perp}$ case should have a higher remanence than in the ZFC case is contradicted by all of the MD samples in this study. In fact the remanence is approximately the same for the $FC_{\parallel}$ and $FC_{\perp}$ cases in spite of the much higher coercivities for the latter.

[24] While the distribution of easy axes certainly has a large effect on the low-temperature magnetic properties of MD magnetite, it does not adequately explain all of the experimental data. Domain wall pinning and nucleation control the coercivity and saturation remanence of MD magnetite [*Dunlop and Özdemir*, 1997]. Indeed, if it were not for these two phenomena, MD magnetite would not display magnetic hysteresis. *Özdemir and Dunlop* [1999] suggested that twin boundaries are important in determining the domain configuration of monoclinic magnetite. Later, *Smirnov and Tarduno* [2002] invoked twinning to explain the so-called field memory effect. Here we apply this idea to our low-temperature experimental results for MD magnetite. Within a single cubic grain, field cooling restricts the *c* axis of the monoclinic phase to the single cube edge closest to the applied field. For ZFC samples a random cube edge becomes the *c* axis of the monoclinic phase; this degree of freedom, if the cubic crystal is large enough, introduces twins. These twins (where two *c* axes meet at right angles)

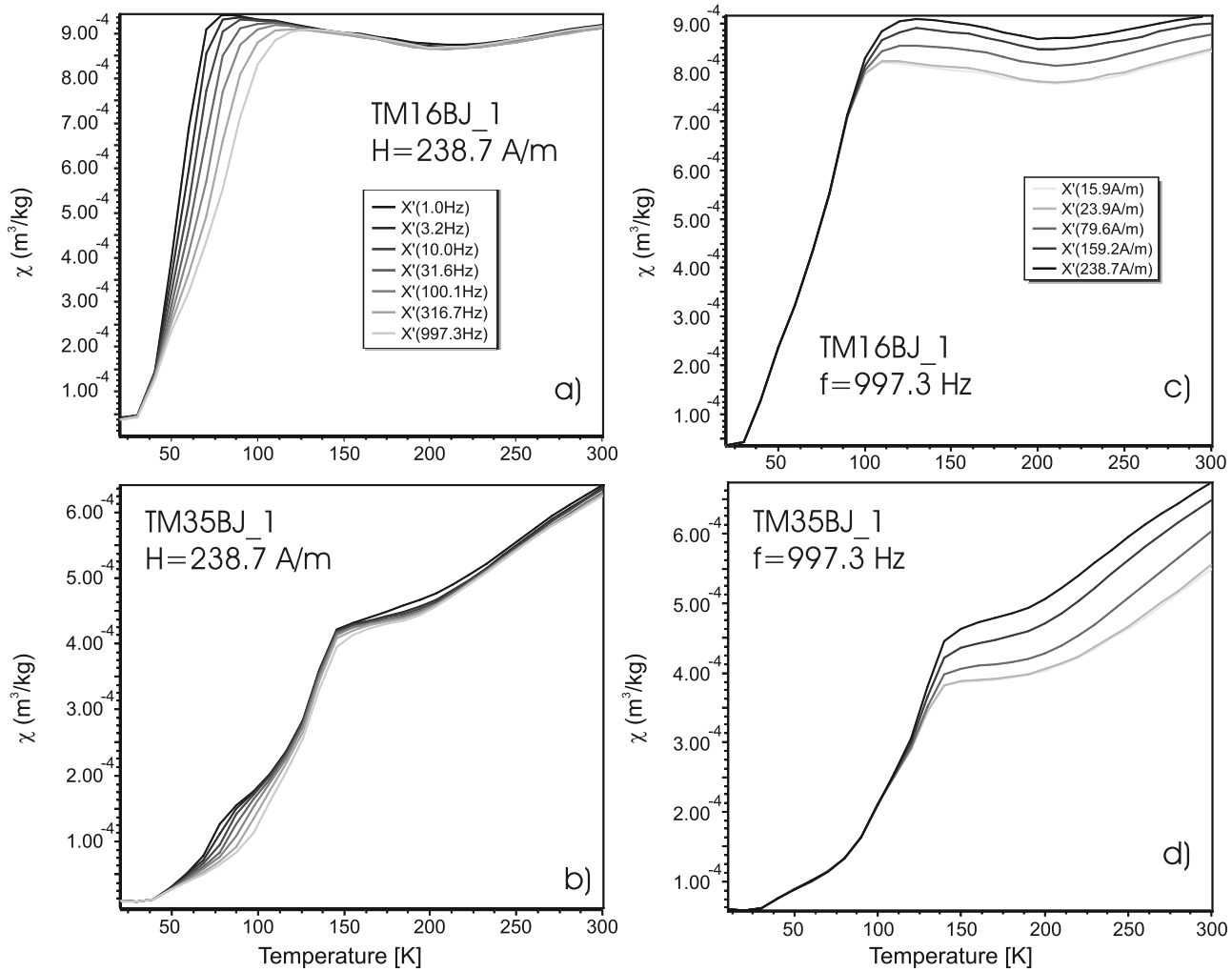

Figure 4. In-phase susceptibility (χ') as a function of temperature and frequency with a constant amplitude (239 A/m) for (a) TM16BJ_1 and (b) TM35BJ_1 and as a function of amplitude and temperature with a constant frequency (997 Hz) for (c) TM16BJ_1 and (d) TM35BJ_1.

are also 90° domain walls because the *c* axes are also the magnetic easy axes. *Moloni et al.* [1996] observed these right angle domain walls in a ZFC single crystal of magnetite using a low-temperature magnetic force microscope (MFM). Figures 5d and 5e show simplified domain patterns for ZFC and FC pretreatment, respectively.

[25] Combining the effect of these monoclinic twins and the geometric effect suggested by *Kosterov* [2003], we are provided with a model that explains all of the observed experimental behavior. The $FC_{\|}$ case is clearly the magnetically softest of the three cases shown in Figure 5; it has both an easy axis bias, where the *c* axis is no more than 55° away from *H*, and easily moved, "soft", 180° domain walls (Figures 5b and 5e). The $FC_{\perp}$ domain walls are easily moved as well (Figure 5f), but courtesy of the distribution of easy axes the wall must be displaced further than in the $FC_{\|}$ case to achieve the same magnetization increase. Thus in small fields the $FC_{\perp}$ case is harder than the $FC_{\|}$ case. As the field increases, however, the domain walls are moved to their limit, and the magnetization can only increase by rotating magnetizations against the hard magnetocrystalline anisotropy. For the $FC_{\perp}$ case this begins at lower fields than the $FC_{\|}$ case. For example moments in the highlighted grain in Figure 5f must rotate against the hard crystalline anisotropy to achieve any increase in magnetization from its remanence state. Thus as the applied field increases, $FC_{\|}$ and $FC_{\perp}$ hysteresis loops should diverge. Of course, for large enough fields even the $FC_{\|}$ magnetizations must begin to rotate, and all three loops, $FC_{\|}$, $FC_{\perp}$, and ZFC should converge to the same saturation magnetization. In the ZFC case, large crystals will be inevitably divided into twins. Within these twins, domain walls will be almost as easily moved as in the $FC_{\|}$ case. However, in order to move a domain wall at a twin boundary the magnetization annexed by the growing domain must immediately be held at a right angle to the easy axis, or alternatively whole domain moments must rotate (Figure 5d). Depending on the balance between these two types of domains the ZFC case would be more or less magnetically hard. Moreover, since cubic crystal twins are likely twins for the low-temperature phase, the degree of polycrystallinity of the cubic phase grains can greatly affect the low-temperature magnetic behavior. In any case, the balance between the hard transformational twin domain walls and the soft 180° domain walls within a single

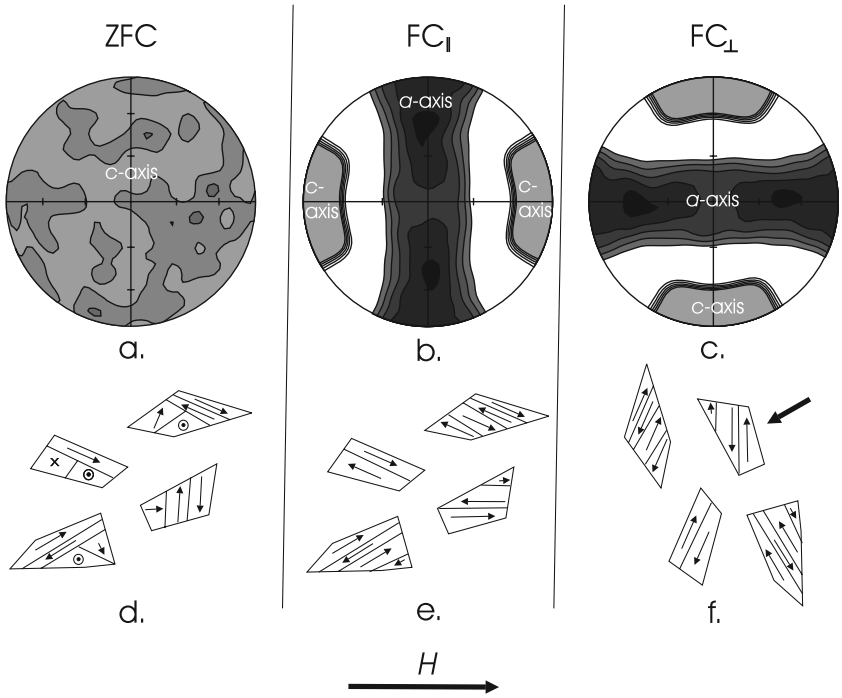

Figure 5. Calculated geometric distributions of (a) *c* axes (magnetic easy axis) of the monoclinic phase for the ZFC case; (b) *c* axes and *a* axes (magnetic hard axis) of the monoclinic phase for the $FC_{||}$ case; (c) *c* axes and *a* axes distribution for the $FC_{\perp}$ case. (d, e, f) Predicted domain patterns for ZFC, $FC_{||}$, and $FC_{\perp}$ cases, respectively.

monoclinic crystal can explain the variation in hardness of the ZFC loops, which are in some cases harder than the $FC_{\perp}$ case and in some cases softer. Since both the ZFC and $FC_{\perp}$ cases have to work against the crystalline anisotropy at lower fields than the $FC_{||}$ case, their magnetizations should converge before they converge with the $FC_{||}$ magnetization (Figures 2a, 2c, 3a, and 3c); this is observed in all four MD samples. The enhanced presence of ultrahard domain wall pinning 90° *c* axis twins in the ZFC case explains its higher remanence ratio and coercive force.

[26] Our domain observations at low-temperature further highlight the effect of transformational twins on magnetite's low-temperature domain configuration. A natural single crystal of magnetite was cut and polished to produce a (100) viewing plane. This is, of course, not the ideal viewing plane for magnetite at room temperature, but below the Verwey transition it is a good choice; for the ZFC case the sample becomes polycrystalline with three *c* axis twin variants: two with *c* axes in the viewing plane, and the third with a *c* axis perpendicular to the viewing plane. In the FC case, a 1.45 T field was applied parallel to one of the in-plane cube edge on cooling.

[27] Figure 6a shows the textures that are consistently visible for the ZFC case. Essentially, there are three types of features: (1) areas of long lamellar domains which are interspersed with strings of circular elements that run parallel to the laths; these laths always run parallel to one of the cube edges and are clearly imaged by the dry Bitter method; (2) large gray areas with little relief, whose perimeters run parallel to the cube edges and can contain a linear pattern which runs parallel to one of the cube edge directions; and (3) areas that contain mottled and convoluted relief.

[28] Feature 1 is entirely consistent with the type of domains observed in a material with strong uniaxial anisotropy whose easy axis is perpendicular to the viewing plane. Specifically we expect such domains for a material where $[1/2(\mu_o M_s^2)]/k_u < 1$ [*Moskowitz et al.*, 1988], where M_s is the saturation magnetization; k_u is the uniaxial anisotropy constant (in the case of monoclinic magnetite the k_a constant from the magnetocrystalline anisotropy is the appropriate number); and μ_o is the permeability of free space. For monoclinic magnetite the ratio is ~3/4. The linear arrangements of circular features are, almost certainly, spike domains. Areas of the sample surface that manifest feature 1 are then twin variants where the *c* axis is perpendicular to the viewing plane. The second feature is more difficult to interpret. Our interpretation is that these features are areas where the body domains' magnetizations lie parallel to viewing plane. We suppose that such domains and their walls are more difficult to image with dry Bitter method since the stray field intensity would be much less than that for body domain magnetizations which are perpendicular to the viewing plane, i.e., in the case of feature 1. As the Fe particles are deposited on the surface they may have too much momentum to effectively reveal such features. Nevertheless, one can make out dim linear features that likely indicate the separations between body domains. Finally, we suspect that feature 3 is the result of residual stresses in the surface that were not completely removed by our final amorphous silica polishing.

[29] The FC textures are much less complicated than those of the ZFC case. In fact, we observe two types of features: (1) long, lamellar, ~10 μm wide domains that are always parallel to the cube edge which was aligned with the cooling field (Figure 6b) and (2) uniform areas with no

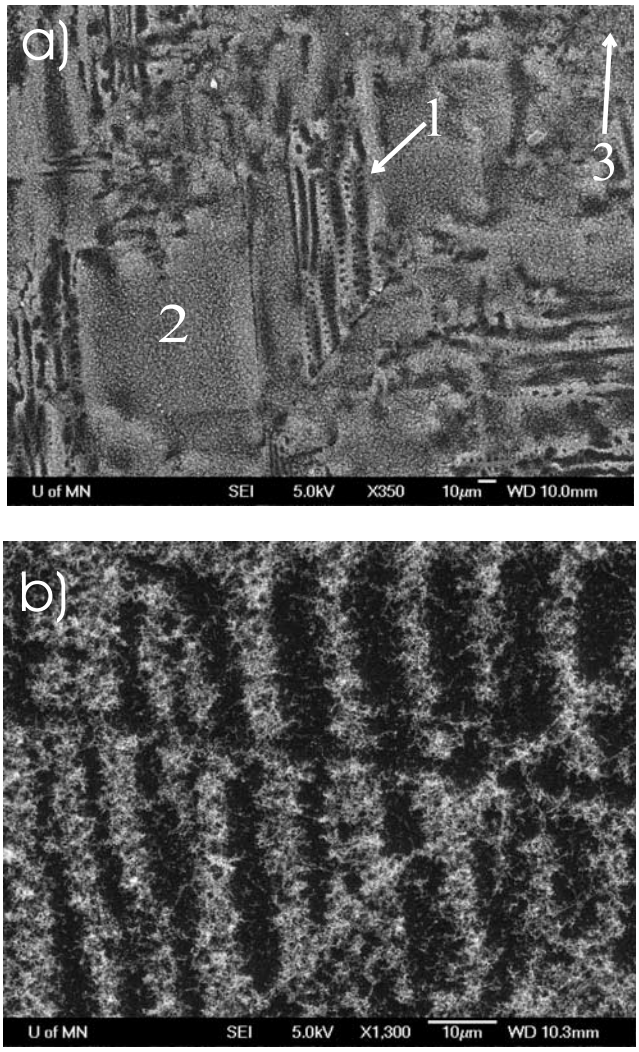

Figure 6. Dry Bitter domain images of a single crystal of magnetite, (100) viewing plane, at 80 K after (a) zero-field cooling and (b) field cooling. The numbers correspond to features described in the text. In both cases, the cube edges are oriented vertically, horizontally, and perpendicular to the plane of the page. For the field-cooled sample the cooling field (1.45 T) was aligned vertically.

relief. The lamellar features are consistent with in-plane domains whose low-temperature easy axis is parallel to the cube edge that was aligned with the cooling field. Again, the uniform areas of coating are likely areas where the domains were not successfully decorated.

[30] We also note that these results are the first characterization of magnetic domain width in monoclinic magnetite, which is on the order of 10 μm.

[31] Comparing Figures 6a and 6b it is easy to imagine how the radically different domain patterns could affect bulk magnetic properties. According to our initial images, the Verwey transition in the ZFC case produces twin domains of $\sim$50 μm in size. This impedes the movement of domain walls, and to the first order, lowers the magnetic grain size of the material, thus, raising the remanent magnetization. For our powder samples of magnetite, the grain size is $\sim$30 μm. If transformational twins play a role in this case, they must be smaller than those observed in the single crystal. *Medrano et al.* [1999] observed long thin twin domains with dimensions of 2 μm by 100 μm. They also suggested "the very probable presence of" twin domains with sizes <5 μm. *Chikazumi et al.* [1970] made similar observations. Further indirect evidence for the occurrence of transformational twins in small MD magnetite is provided by *Smirnov*'s [2006] interpretation of the so-called field memory effect. We are planning domain observations that will constrain the twin configuration of small MD grains.

4.2. TM16 and TM35

[32] The similarities in magnetic behavior of the magnetite and titanomagnetites characterized in this study are striking. All three show: large drops in magnetization on warming through a critical temperature (T_v for magnetite); elevated ZFC remanences over FC remanences below the critical temperature; and large increases in magnetic susceptibility on warming through the critical temperature. It is equally interesting to note a major difference between the titanomagnetite data and the magnetite data: the frequency dependence of susceptibility for the titanomagnetites near T_{crit}. For the titanomagnetites, the transition temperature (as it is manifested in magnetic measurements) increases with decreasing timescale of the magnetic measurement. This strongly suggests a thermally activated process. Specifically, the magnetic after effect observed between $\sim$50 and 100 K is thought to be related to thermally activated electron hopping [*Walz et al.*, 1997].

[33] Assuming a thermally activated process that follows an Arrhenius equation, we plotted ln(1/*f*) versus the transition temperature as deduced from our susceptibility measurements (Figure 7). The *f* is the frequency of the applied field during the susceptibility measurement, and the transition temperature was taken as the peak in the temperature derivative of magnetic susceptibility. The data fall on a line, whose slope (equal to Q/k) gives an activation energy, Q, of $\sim$0.1 eV, consistent with a thermally activated electron hopping process [*Kronmüller and Walz*, 1980; *Brabers*, 1995; *Walz et al.*, 2003].

[34] We also measured Mössbauer spectra for TM16BJ_1 at 300 K and 4.2 K. The room temperature spectrum is composed of two sextets each with a distribution of hyperfine fields (Figure 8 and Table 2). The first is consistent with tetrahedrally coordinated A site Fe^{+3} and was characterized by a narrow distribution of hyperfine fields. The second sextet is generated by the octahedral B site iron, which due to electron hopping between Fe^{+3} and Fe^{+2}, is effectively $Fe^{+2.5}$. Since Ti substitutes on the B site, it is not surprising that B site iron yields a broad distribution of hyperfine fields, while the A site iron does not [*Banerjee et al.*, 1966]. The proportions of sextet 1 (the tetrahedral iron) and sextet 2 (the octahedral iron) are 32% and 68%, respectively. For titanomagnetites with $x < 0.2$ little to no Fe^{+2} is expected to occur in tetrahedrally coordinated A sites [*O'Reilly and Banerjee*, 1965; *Kakol et al.*, 1991a]. This is consistent with our Mössbauer spectra.

[35] At 4.2 K two sextets are, again, clearly present. At low temperature, however, the proportions are now reversed: the sextet with the larger hyperfine field encompasses 66% of the total spectrum while the other is only

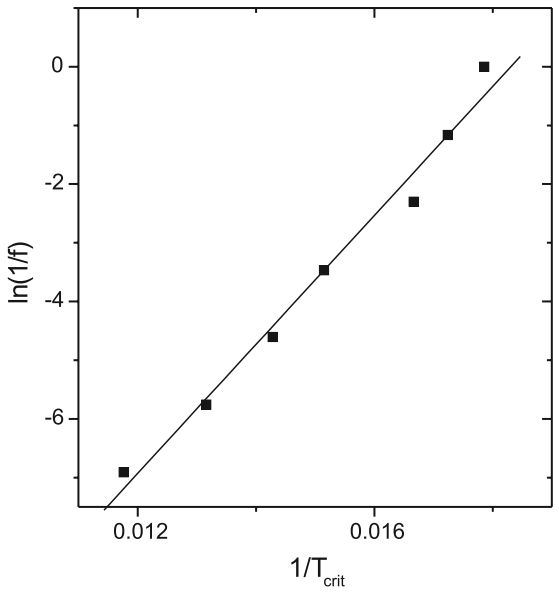

Figure 7. The ln(1/f) versus $1/T_{crit}$ as deduced from susceptibility measurements for TM16BJ_1.

34%. This switch is consistent with the suppression of electron hopping within the B site, at least on the timescale of the Mössbauer measurement. If correct, at low-temperature the Mössbauer spectrum is influenced by three distinct iron cations: tetrahedral Fe^{+3}, octahedral Fe^{+3}, and octahedral Fe^{+2}. Both Fe^{+3} coordinations should generate strongly overlapping sextets with similar magnetic hyperfine field, quadrupole splitting and isomer shift, which are fit with a single sextet (Figure 8 (top) and Table 2) [*Murad and Cashion*, 2004]. The second sextet with the smaller hyperfine field is, then, due to only the B site Fe^{+2}. The suppression of electron hoping is thus consistent with the variable temperature Mössbauer data.

[36] The gradual suppression of electron hopping at low temperatures is most likely the controlling process driving the observed magnetic behavior across T_{crit} for our samples of TM16 and TM35. Specifically, when the timescale of the electron hopping becomes longer than the timescale of the magnetic experiment, the effect on the measured magnetic parameter becomes evident. As pointed out by *Schmidbauer and Readman* [1982] below T_{crit} a new grain-scale magnetic anisotropy must be present. We now suggest that this anisotropy is related to the suppression of thermally activated electron hopping and the localization of anisotropic Fe^{+2} ions in octahedral coordination. In terms of the susceptibility data, the anisotropy causes a decrease in wall mobility, a drop in susceptibility and suppression of amplitude dependence of susceptibility below T_{crit}. Furthermore, unlike in magnetite, where electron hopping ceases abruptly (at all timescales) at the Verwey transition, the transition in titanomagnetites does not seem to be discontinuous. In terms of the magnetic measurements, the temperature at which the hard low-temperature anisotropy is first observed is a function of the timescale of the magnetic measurement. This is consistent with electrical conductivity measurements at low temperatures which also do not show a discontinuous change [*Brabers*, 1995].

[37] *Schmidbauer and Readman* [1982] also demonstrated that the orientation of the easy axis of the low-temperature anisotropy, which they suggested was uniaxial, could be controlled by a magnetic field. Our remanence measurements show a similar effect; we observe, however, elevated ZFC remanences over FC ones, whereas they observed the opposite. We note that *Schmidbauer and Readman* [1982] obtained their data by measuring hysteresis loops as a function of temperature with a maximum applied field of 1.45 T. Undersaturated ZFC loops might explain the discrepancy between their data and ours. In order to explain our ZFC/FC results, we appeal to the same process as we did for magnetite. Given a single crystal of titanomagnetite, on cooling through the transition in a zero field, one volume of the grain may adopt an easy axis in one direction, while another volume may adopt a different orientation. The boundaries between these volumes are natural locations for domain walls and potent pinning sites. In the FC case, the easy axis is restricted, and such contacts are reduced in number or eliminated completely depending on the degree of field control.

[38] Finally, we predict that single domain grains of titanomagnetite will only contain one anisotropy orientation and will thus produce FC remanences which are

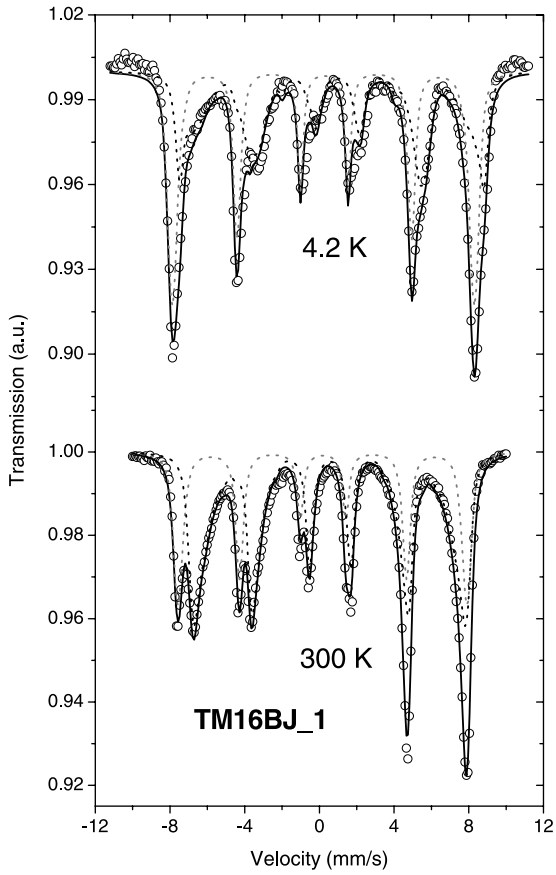

Figure 8. Mössbauer spectra for TM16BJ_1 at 4.2 K and 300 K. Sextet 1 is shown as a dashed gray line, sextet 2 is shown as a dashed black line, and the sum of the two is shown as a solid black line.

Table 2. Mössbauer Hyperfine Parameters at Room Temperature and 4.2 K for Sample TMBJ16_1[a]

	Sextet 1				Sextet 2			
	B_{HF}, T	Δ, mm/s	δ, mm/s	Percent	B_{HF}, T	Δ, mm/s	δ, mm/s	Percent
300 K	48.0(1)	−0.03(2)	0.31(1)	32	45.5(1)	−0.03(1)	0.69(1)	68
4.2 K	50.0(2)	−0.07(1)	0.37(1)	66	47.0(1)	−0.27(1)	1.07(1)	34

[a]At 300 K sextet 1 is produced by the Fe^{3+} tetrahedral site and sextet 2 is produced by the $Fe^{+2.5}$ octahedral site. At 4.3 K, both Fe^{+3} coordinations contribute to sextet 1, while sextet 2 is due to only the Fe^{+2}. Maximum hyperfine field (B_{HF}), quadrupole splitting (Δ), isomer shift (δ). Errors are quoted within parentheses.

more intense than ZFC ones, similar to single domain magnetite.

[39] Note that we are not suggesting that a change in crystal structure necessarily occurs. As the electron hopping becomes increasingly sluggish at low temperatures, the octahedral iron may or may not order in the octahedral B site and may or may not induce a change in crystal structure.

5. Conclusions

[40] The low-temperature magnetic properties of the MD magnetite and titanomagnetites characterized in this study can be summarized in the following way: ZFC remanences are elevated above FC remanences at low temperature for both magnetite and titanomagnetites, at least up to $x \sim 0.35$. Thus the elevation of ZFC remanences over FC remanences is diagnostic of the presence of MD titanomagnetites, with $0 < x < \sim 0.35$. This difference between FC and ZFC remanences is most likely caused by domain wall pinning boundaries between volumes within a grain with different anisotropy orientations. Such boundaries are present in the ZFC case but greatly reduced or absent in the FC case. In the case of magnetite, it is the Verwey transition and associated transformation twins which produce such boundaries. Our low-temperature magnetic domain observations in magnetite support this theory, and provide the first direct constraints on the magnetic domain configuration of monoclinic magnetite. In the case of the titanomagnetites, we suppose that the boundaries are produced as a new low-temperature magnetic anisotropy is induced. We further surmise that titanomagnetite's low-temperature anisotropy is observed when the characteristic time of electron hopping within the octahedral B site (which becomes increasingly sluggish at low temperatures) slows to the timescale of the magnetic measurement. T_{crit} itself, e.g., deduced from remanence measurements, is also useful in differentiating magnetite from titanomagnetites.

[41] **Acknowledgments.** IRM is supported by the Instrumentation and Facilities Program, Earth Science Division, National Science Foundation. Finally, we thank Ö. Özdemir and A. Muxworthy for their helpful and insightful reviews. This is IRM contribution 0606.

References

Banerjee, S. K., C. P. Hunt, and X.-M. Liu (1993), Separation of local signals from the regional paleomonsoon record of the Chinese loess plateau: A rock-magnetic approach, *Geophys. Res. Lett.*, *20*, 843–846.

Banerjee, S. K., W. O'Reilly, T. C. Gibb, and N. N. Greenwood (1966), Influence on hyperfine field of local variations in inverse spinels, *Phys. Lett.*, *20*, 455–457.

Bogalo, M. F., F. Heller, and M. L. Osete (2001), Isothermal remanence experiments at room and at liquid nitrogen temperature: Application to soil studies, *Geophys. Res. Lett.*, *28*, 419–422.

Brabers, V. A. M. (1995), The electrical conduction of titanomagnetites, *Physica B*, *205*(2), 143–152.

Brachfeld, S., Y. Guyodo, and G. D. Acton (2001), The magnetic mineral assemblage of hemipelagic drifts, ODP Site 1096, *Ocean Drill. Program Sci. Results*, *178* [Online]. (Available at http://www.odp.tamu.edu/publications/178_SR/VOLUME/CHAPTERS/SR178_14.PDF).

Brachfeld, S. A., S. K. Banerjee, Y. Guyodo, and G. D. Acton (2002), A 13200 year history of century to millennial-scale paleoenvironmental change magnetically recorded in the Palmer Deep, western Antarctic Peninsula, *Earth Planet. Sci. Lett.*, *194*, 311–326.

Carter-Stiglitz, B., B. Moskowitz, and M. Jackson (2001), Unmixing magnetic assemblages and the magnetic behavior of bimodal mixtures, *J. Geophys. Res.*, *106*(B11), 26,397–26,412.

Carter-Stiglitz, B., M. Jackson, and B. Moskowitz (2002), Low-temperature remanence in stable single domain magnetite, *Geophys. Res. Lett.*, *29*(7), 1129, doi:10.1029/2001GL014197.

Chikazumi, S., K. Chiba, K. Suzuki, and T. Yamada (1970), Electron microscopic observation of low temperature phase of magnetite, in *Ferrites: Proceedings of the International Conference*, edited by Y. Hoshino, S. Iida, and M. Sugimoto, pp. 595–597, University Park Press, Baltimore, Md.

Creer, K. M., and C. B. Like (1967), A low temperature investigation of the natural remanent magnetization of several igneous rocks, *Geophys. J. R. Astron. Soc.*, *12*(3), 301–312.

Dearing, J. A., P. M. Bird, R. J. L. Dann, and S. F. Benjamin (1997), Secondary ferrimagnetic minerals in Welsh soils: A comparison of mineral magnetic detection methods and implications for mineral formation, *Geophys. J. Int.*, *130*, 727–736.

Dunlop, D. J., and K. S. Argyle (1991), Separating multidomain and single-domain-like remanences in pseudo-single-domain magnetites (215–540 nm) by low-temperature demagnetization, *J. Geophys. Res.*, *96*, 2007–2017.

Dunlop, D. J., and Ö. Özdemir (1997), *Rock Magnetism: Fundamentals and Frontiers*, 573 pp., Cambridge Univ. Press, New York.

Eyre, J. K., and J. Shaw (1994), Magnetic enhancement of Chinese loess—The role of γ-Fe_2O_3?, *Geophys. J. Int.*, *117*, 265–271.

Halgedahl, S. L., and R. D. Jarrard (1995), Low-temperature behavior of single domain through multidomain magnetite, *Earth Planet. Sci. Lett.*, *130*, 127–139.

Heider, F., D. J. Dunlop, and H. C. Soffel (1992), Low-temperature and alternating field demagnetization of saturation remanence and thermoremanence in magnetite grains (0.37 μm to 5 mm), *J. Geophys. Res.*, *97*, 9371–9381.

Hodych, J. P. (1991), Low-temperature demagnetization of saturation remanence in rocks bearing multidomain magnetite, *Phys. Earth Planet. Inter.*, *66*, 144–152.

Hunt, C. P., S. K. Banerjee, J.-M. Han, P. A. Solheid, E. A. Oches, W.-W. Sun, and T.-S. Liu (1995), Rock-magnetic proxies of climate change in the loess-paleosol sequences of the western Loess Plateau of China, *Geophys. J. Int.*, *123*, 232–244.

Jackson, M. J., H.-U. Worm, and S. K. Banerjee (1990), Fourier analysis of digital hysteresis data: Rock magnetic applications, *Phys. Earth Planet. Inter.*, *65*, 78–87.

Jackson, M. J., P. Rochette, G. Fillion, S. K. Banerjee, and J. A. Marvin (1993), Rock magnetism of remagnetized Paleozoic carbonates: Low-temperature behavior and susceptibility characteristics, *J. Geophys. Res.*, *98*, 6217–6225.

Jackson, M., B. Moskowitz, J. Rosenbaum, and C. Kissel (1998), Field-dependence of AC susceptibility in titanomagnetites, *Earth Planet. Sci. Lett.*, *157*, 129–139.

Kakol, Z., J. Sabol, and J. M. Honig (1991a), Cation distribution and magnetic properties of titanomagnetites $Fe_{3-x}Ti_xO_4 (0 < x < 1)$, *Phys. Rev. B*, *43*, 649–654.

Kakol, Z., J. Sabol, and J. M. Honig (1991b), Magnetic anisotropy of titanomagnetites $Fe_{3-x}Ti_xO_4$, $0 < x < 0.55$, *Phys. Rev. B*, *44*, 2198–2204.

King, J. G., and W. Williams (2000), Low-temperature magnetic properties of magnetite, *J. Geophys. Res.*, *105*, 16,427–16,436.

Kosterov, A. (2001), Magnetic hysteresis of pseudo-single-domain and multidomain magnetite below the Verwey transition, *Earth Planet. Sci. Lett.*, *186*, 245–254.

Kosterov, A. (2002), Low-temperature magnetic hysteresis properties of partially oxidized magnetite, *Geophys. J. Int.*, *149*(3), 796–804.

Kosterov, A. (2003), Low-temperature magnetization and AC susceptibility of magnetite: Effect of thermomagnetic history, *Geophys. J. Int.*, *154*(1), 58–71.

Kronmüller, H., and F. Walz (1980), Magnetic after-effects in Fe_3O_4 and vacancy-doped magnetite, *Philos. Mag. B*, *42*(3), 433–452.

Kronmüller, H., R. Schützenauer, and F. Waltz (1974), Magnetic aftereffects in magnetite, *Phys. Status Solidi A*, *24*, 487–494.

Li, C. H. (1932), Magnetic properties of magnetite crystals at low temperature, *Phys. Rev.*, *40*, 1002–1012.

Medrano, C., M. Schlenker, J. Baruchel, J. Espeso, and Y. Miyamoto (1999), Domains in the low-temperature phase of magnetite from synchrotron-radiation X-ray topographs, *Phys. Rev. B*, *59*(2), 1185–1195.

Moloni, K., B. M. Moskowitz, and E. D. Dahlberg (1996), Domain structures in single crystal magnetitite below the Verwey transition as observed with a low-temperature magnetic force microscope, *Geophys. Res. Lett.*, *23*, 2851–2854.

Moskowitz, B. M., S. L. Halgedahl, and C. A. Lawson (1988), Magnetic domains on unpolished and polished surfaces of titanium-rich titanomagnetite, *J. Geophys. Res.*, *93*, 3372–3386.

Moskowitz, B. M., R. Frankel, and D. Bazylinski (1993), Rock magnetic criteria for the detection of biogenic magnetite, *Earth Planet. Sci. Lett.*, *120*, 283–300.

Moskowitz, B. M., M. Jackson, and C. Kissel (1998), Low-temperature magnetic behavior of titanomagnetites, *Earth Planet. Sci. Lett.*, *157*, 141–149.

Murad, E., and J. Cashion (2004), *Mossbauer Spectroscopy of Environmental Material and Their Industrial Utilization*, Springer, New York.

Muxworthy, A. R., and E. McClelland (2000), The causes of low-temperature demagnetization of remanence in multidomain magnetite, *Geophys. J. Int.*, *140*(1), 115–131.

Muxworthy, A. R., and W. Williams (1999), Micromagnetic models of pseudo-single domain grains of magnetite near the Verwey transition, *J. Geophys. Res.*, *104*, 29,203–29,217.

Nagata, T. (1965), Low temperature characteristics of rock magnetism, *J. Geomagn. Geoelectr.*, *17*, 315–324.

O'Reilly, W., and S. K. Banerjee (1965), Cation distribution in titanomagnetites $(1-x)\ Fe_3O_4-x\ Fe_2TiO_4$, *Phys. Lett.*, *17*, 237–238.

Özdemir, Ö., and D. J. Dunlop (1999), Low-temperature properties of a single crystal of magnetite oriented along principal magnetic axes, *Earth Planet. Sci. Lett.*, *165*, 229–239.

Özdemir, Ö., D. J. Dunlop, and B. M. Moskowitz (1993), The effect of oxidation on the Verwey transition in magnetite, *Geophys. Res. Lett.*, *20*, 1671–1674.

Özdemir, Ö., D. J. Dunlop, and B. M. Moskowitz (2002), Changes in remanence, coercivity and domain state at low temperature in magnetite, *Earth Planet. Sci. Lett.*, *194*, 343–358.

Ozima, M., M. Ozima, and S. Akimoto (1964), Low temperature characteristics of remanent magnetization of magnetite—Self-reversal and recovery phenomena of remanent magnetization, *J. Geomagn. Geoelectr.*, *16*, 165–177.

Passier, H. F., G. J. de Lange, and M. J. Dekkers (2001), Magnetic properties and geochemistry of the active oxidation front and the youngest sapropel in the eastern Mediterranean Sea, *Geophys. J. Int.*, *145*(3), 604–614.

Radhakrishnamurty, C., and S. D. Likhite (1993), Frequency dependence of low-temperature susceptibility peak in some titanomagnetites, *Phys. Earth Planet. Inter.*, *76*, 131–135.

Roberts, A. P., Y.-L. Cui, and K. L. Verosub (1995), Wasp-waisted hysteresis loops: Mineral magnetic characteristics and discrimination of components in mixed magnetic systems, *J. Geophys. Res.*, *100*, 17,909–17,924.

Rochette, P., G. Fillion, J.-L. Mattéi, and M. J. Dekkers (1990), Magnetic transition at 30–34 Kelvin in pyrrhotite: Insight into a widespread occurrence of this mineral in rocks, *Earth Planet. Sci. Lett.*, *98*, 319–328.

Schmidbauer, E., and P. W. Readman (1982), Low temperature magnetic properties of Ti-rich Fe-Ti spinels, *J. Magn. Magn. Mater.*, *27*, 114–118.

Shcherbakova, V. V., V. P. Shcherbakov, P. W. Schmidt, and M. Prévot (1996), On the effect of low-temperature demagnetization on TRMs and pTRMs, *Geophys. J. Int.*, *127*(2), 379–386.

Skumryev, V., H. J. Blythe, J. Cullen, and J. M. D. Coey (1999), AC susceptibility of a magnetite crystal, *J. Magn. Magn. Mater.*, *196*, 863–864.

Smirnov, A. V. (2006), Memory of the magnetic field applied during cooling in the low-temperature phase of magnetite: Grain size dependence, *J. Geophys. Res.*, *111*, B12S04, doi:10.1029/2006JB004573.

Smirnov, A. V., and J. A. Tarduno (2002), Magnetic field control of the low-temperature magnetic properties of stoichiometric and cation-deficient magnetite, *Earth Planet. Sci. Lett.*, *194*, 359–368.

Smith, R. L., W. D. Corner, and B. K. Tanner (1980), An apparatus for observing magnetic domains at low temperatures and in large applied fields., *J. Phys. E*, *13*(6), 620–622.

Syono, Y. (1965), Magnetocrystalline anisotropy and magnetostriction of $Fe_3O_4-Fe_2TiO_4$ series, with special application to rock magnetism, *Jpn. J. Geophys.*, *4*, 71–143.

Tarduno, J. A. (1995), Superparamagnetism and reduction diagenesis in pelagic sediments: Enhancement or depletion?, *Geophys. Res. Lett.*, *22*, 1337–1340.

Torii, M., K. Fukuma, C.-S. Horng, and T.-Q. Lee (1996), Magnetic discrimination of pyrrhotite- and greigite-bearing sediment samples, *Geophys. Res. Lett.*, *23*, 1813–1816.

Walz, F., L. Torres, K. Bendimya, C. de Francisco, and H. Kronmüller (1997), Analysis of magnetic after-effect spectra in titanium-doped magnetite, *Physica Status Solidi A*, *164*, 805–20.

Walz, F., V. A. M. Brabers, J. H. V. J. Brabers, and H. Kronmüller (2003), Stress-induced relaxation mechanisms in single-crystalline titanomagnetites, *J. Phys. Condens. Matter*, *15*(41), 7029–7045.

Wanamaker, B. J., and B. M. Moskowitz (1994), Effect of nonstoichiometry on the magnetic and electrical properties of synthetic single crystal $Fe_{2.4}Ti_{0.6}O_4$, *Geophys. Res. Lett.*, *21*, 983–986.

Yu, Y., D. J. Dunlop, and Ö. Özdemir (2002), Partial anhysteretic remanent magnetization in magnetite: 1. Additivity, *J. Geophys. Res.*, *107*(B10), 2244, doi:10.1029/2001JB001249.

T. S. Berquó, B. Carter-Stiglitz, M. Jackson, A. Kosterov, B. Moskowitz, and P. Solheid, Institute for Rock Magnetism, Newton Horace Winchell School of Earth Sciences, University of Minnesota, 291 Shepherd Lab., 100 Union St. SE, Minneapolis, MN 55455, USA. (cart0196@tc.umn.edu)